no appreciable angular acceleration of the ring in the initial phase of each test, an indication that the fragments readily slid along the inside surface. A triangular radial velocity distribution acting over three ring segments of eleven masses each was then assumed as shown in Fig. 2. This tentative distribution was chosen on the basis of the apparent contact area shown in the high-speed photographs.

In order to calculate an initial velocity value for the mass points, an elastic collision was assumed. Conservation of linear momentum, angular momentum, and kinetic energy before and after collision yields the following three equations with three unknowns:

$$M_f V_0 = M_f V_f + m \sum_{j=1}^{11} ju$$

$$I_f \omega_0 = I_f \omega_f + ma \sum_{j=1}^{11} ju \qquad (4)$$

$$\tfrac{1}{2} M_f V_0^2 + \tfrac{1}{2} I_f \omega_0^2 = \tfrac{1}{2} M_f V_f^2 + \tfrac{1}{2} I_f \omega_f^2 + \tfrac{1}{2} m \sum_{j=1}^{11} (ju)^2$$

where V = fragment centroidal velocity normal to the ring, the incremental velocity u and the quantity a are defined in Fig. 2; the subscripts o and f on V and ω indicate before and after collision, respectively. When these equations are solved simultaneously, the following equation for the incremental velocity u is obtained:

$$u = 132(V_0 + a\omega_0)/[4356(m/M_f + a^2 m/I_f) + 506] \qquad (5)$$

The resulting error in momentum incurred by choosing the imparted velocity direction to be radial at each mass point, rather than the single fragment direction, was neglected.

Results

The value of the predicted shear stress occurring at the point of impact vs time, obtained from the JET 1 analysis, is plotted in Fig. 3 for each of the two test cases. The maximum shear stress value obtained for the run in which the ring failed was 92,300 psi, which substantially exceeds the Ref. 4 value of the ultimate shear stress for 4130 steel. The maximum shear-stress value obtained for the run in which the ring did not fail was 65,220 psi, which was considerably below the ultimate shear-stress value.

Strain rate effects were not included in the analysis because data for 4130 steel at high strain rates were not available. Although this omission significantly affects the maximum value of shear stress obtained, the fact that the static value of ultimate shear stress was used to test for failure makes the analysis consistent.

From Fig. 3, the calculated time to failure for case 1 is seen to occur within 1 μsec after impact, whereas the ring failure is evident in the high-speed photographs only after approximately 400 μsec. Part of this rather large discrepancy can be explained by the fact that the gap in the ring when failure was first detected from the photographs is on the order of $\frac{1}{2}$ in., and since the initial ring mass-point velocity at the impact point is approximately 5000 in./sec, it will take over 100 μsec for a failure to be detectable for this reason alone.

Conclusions

The present initial results of this continuing study indicate that containment rings may be shear failure critical if certain types of fragments are used. In addition to the previously described nondeforming type of fragment, fragments of interest could include those from the large-diameter fan blades incorporated in the new generation high mass-flow jet engines to be used on "Jumbo Jet" type aircraft. When analyses are made similar to those described here, care must be exercised that enough mass increments are used to obtain convergent values of shear stress. Although applicable to other types of fragments in a general way, the aforementioned impulse calculation should obviously be used in its present form only for nondeforming fragments, since the energy used to deform bladed rotors will decrease, to some degree, the amount of energy transferred to the ring. Finally, the results indicate that perhaps a new nondeforming fragment, possibly with rounded edges, can be found which better simulates the types of ring response that have been obtained from bladed rotor interaction tests.

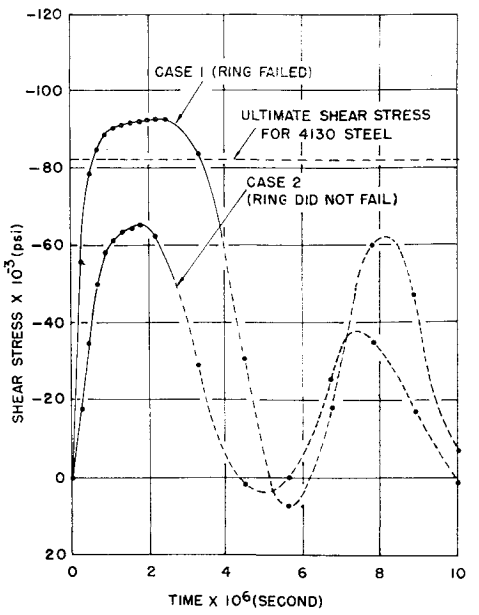

Fig. 3 Calculated shear stress at each impact point vs time.

References

[1] McCallum, R. B., Leech, J. W., and Witmer, E. A., "Progress in the Analysis of Jet Engine Burst-Rotor Containment Devices," ASRL TR 154-1, Aug. 1969, Aeroelastic and Structures Research Lab., Massachusetts Institute of Technology.

[2] Witmer, E. A. et al., "Large Dynamic Deformations of Beams, Rings, Plates, and Shells," *AIAA Journal*, Vol. 1, No. 8, Aug. 1963, pp. 1848–1857.

[3] Leech, J. W., Witmer, E. A., and Pian, T. H. H., "Numerical Calculation Technique for Large Elastic-Plastic Transient Deformations of Thin Shells," *AIAA Journal*, Vol. 6, No. 12, Dec. 1968, pp. 2352–2359.

[4] "Strenth of Metal Aircraft Elements," *Military Handbook*, MIL-HDBK-5, March 1959, Armed Forces Supply Support Center, Washington D.C.

Critical Preston-Tube Sizes

JERRY M. ALLEN*
NASA Langley Research Center, Hampton, Va.

Nomenclature†

C_f = local skin-friction coefficient
C_F = average skin-friction coefficient
d = Preston-tube diameter

Received October 30, 1969.

* Aerospace Engineer, Full-Scale Research Division. Member AIAA.

† Primed quantities are evaluated at reference temperature.

M = Mach number
R_x = Reynolds number based on x
R_θ = Reynolds number based on θ
t = ratio of inside to outside diameter of probe
T = absolute temperature
u = velocity in x direction
x = streamwise coordinate
y = normal coordinate
δ = boundary-layer thickness
θ = boundary-layer momentum thickness
μ = viscosity
ρ = density

Subscripts

max = maximum
min = minimum
e = local freestream

CURVES for estimating the maximum and minimum allowable Preston-tube diameters have been presented in Ref. 1 by Hopkins and Keener. These curves allow the determination of an acceptable probe size in flat-plate flow if the freestream conditions and distance from the measuring station to the origin of turbulent flow are known.

The premise on which these limits are based is that the Preston-tube measurement should be made in the logarithmic region of the boundary layer. The maximum size limit originated from Fenter and Stalmach in Ref. 2 from experimental observations of the point at which velocity profiles began to deviate significantly from the logarithmic law. This point is given in Ref. 2 as

$$y_{max}/\delta = 0.3 \tag{1}$$

If it is assumed that the probe size is such that y_{max} extends to the top of the probe opening, then d_{max} and y_{max} can be related

$$y_{max} = d_{max}(t + 1)/2 \tag{2}$$

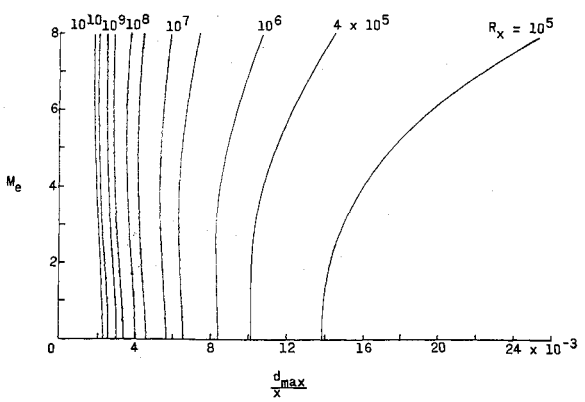

Fig. 1a) Critical Preston-tube sizes—maximum.

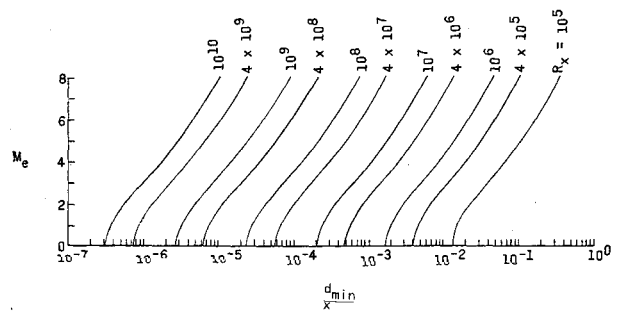

Fig. 1b) Minimum.

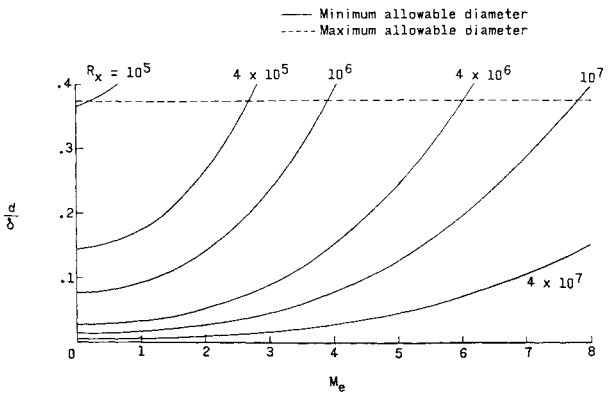

Fig. 2 Effect of Mach and Reynolds numbers on critical-tube sizes.

Combining Eqs. (1) and (2), and making use of $C_F = 2\theta/x$ yields for $t = 0.6$,

$$d_{max}/x = 0.1875\, C_F/(\theta/\delta) \tag{3}$$

The minimum size limit is given by Hopkins and Keener as

$$\rho_e u_e d_{min}/\mu_e = 100/C_f^{0.5}(\mu_e/\mu')(\rho'/\rho_e)^{0.5} \tag{4}$$

which was obtained from the point at which experimental Preston-tube data began to deviate from their linear calibration. Using the power-law viscosity-temperature relationship, $\mu_e/\mu' = (T_e/T')^{0.768}$, and Sommer and Short's reference temperature for adiabatic walls, $T'/T_e = 1 + 0.1142M_e^2$, in Eq. (4) results in

$$d_{min}/x = 100(1 + 0.1142M_e^2)^{1.268}/R_x C_f^{0.5} \tag{5}$$

Figure 1 shows the maximum and minimum diameter curves calculated by Eqs. (3) and (5) using flat-plate theory to estimate the viscous quantities. The minimum diameter curves are identical to the ones given by Hopkins and Keener, while the maximum diameter curves differ slightly because of Hopkins and Keener's slightly different application of the Fenter-Stalmach criterion $y_{max}/\delta = 0.3$.

It should be noted that under some flow conditions, namely, high Mach number and low Reynolds number, the maximum allowable diameter is smaller than the minimum allowable diameter. This can be more easily seen with the aid of Fig. 2, which contains the same maximum and minimum criterion shown in Fig. 1 plotted in a different form.

It can be seen that at the higher Reynolds numbers, the minimum allowable diameter remains relatively small with increasing Mach number, but a rapid increase in minimum size occurs at the lower Reynolds numbers. Beyond the point at which the maximum and minimum curves intersect, there is, of course, no probe size which could be successfully used as a Preston tube. This, in effect, means that under those flow conditions, there is no logarithmic portion of the boundary layer.

Plotting the intersection of these curves yields Fig. 3, which can be used as a quick and easy check to see if the Preston-

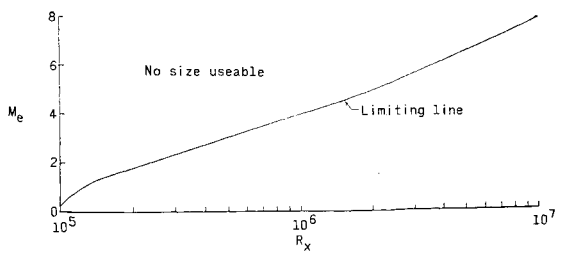

Fig. 3 Preston-tube critical size limiting line.

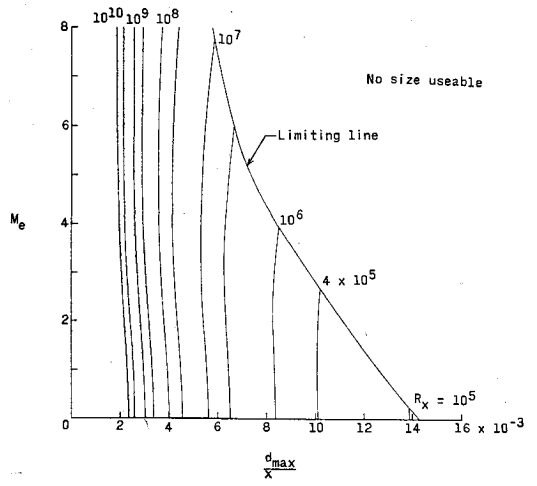

Fig. 4a) Critical Preston-tube sizes including limiting line—maximum.

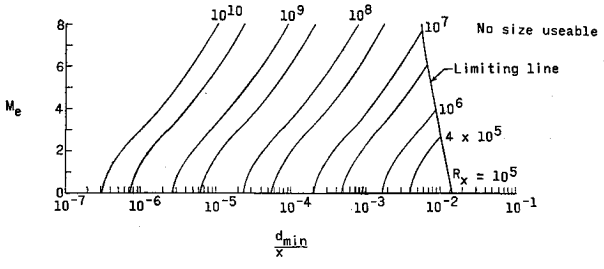

Fig. 4b) Minimum.

tube technique can be successfully used at the test conditions of interest.

To be internally consistent, therefore, the curves in Fig. 1 should appear as in Fig. 4, where the no-useable-size areas have been removed.

In cases where the length of turbulent flow is not known, such as experiments on wind-tunnel sidewalls, the critical-size curves presented in terms of x would not be useful. If the local momentum thickness were known, however, probe-size estimates could still be made by replacing x in Eqs. (3)

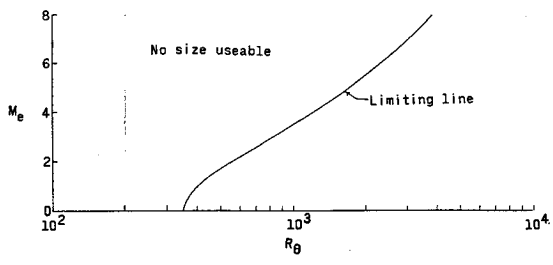

Fig. 5 Limiting line in terms of momentum thickness.

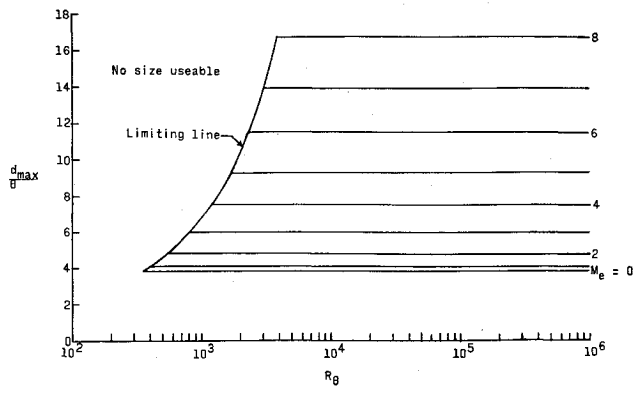

Fig. 6a) Critical Preston-tube sizes in terms of momentum thickness—maximum.

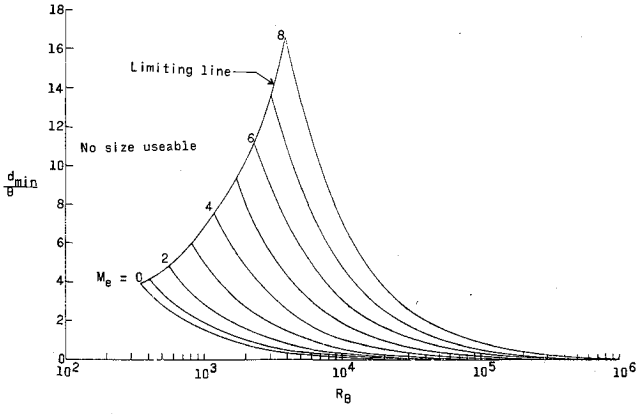

Fig. 6b) Minimum.

and (5) by $2\theta/C_F$. These equations then become

$$d_{max}/\theta = 0.375/(\theta/\delta) \tag{6}$$

and

$$d_{min}/\theta = 100(1 + 0.1142M_e^2)^{1.268}/R_\theta C_f^{0.5} \tag{7}$$

Probe-size limits can now be made in terms of momentum thickness. Figure 5 shows the limiting line curve obtained from Fig. 4, and the curves derived from Eqs. (6) and (7) are shown in Fig. 6.

References

[1] Hopkins, E. J. and Keener, E. R., "Study of Surface Pitots for Measuring Turbulent Skin Friction at Supersonic Mach Numbers—Adiabatic Wall," TN D-3478, 1966, NASA.

[2] Fenter, F. W. and Stalmach, C. J., "The Measurement of Local Turbulent Skin Friction at Supersonic Speeds by Means of Surface Impact Pressure Probes," DRL 392, CM 878, 1957, Univ. of Texas.